Observation of Elemental Anomalies at the Surface of Palladium after Electrochemical Loading of Deuterium or Hydrogen

Debra R. Rolison* and William E. O'Grady

Surface Chemistry Branch, Code 6170, Naval Research Laboratory, Washington, D.C. 20375-5000

In this work, the results from surface-sensitive analyses are reported for Pd after electrolysis of light water and heavy water. Pd foils used to electrolyze D_2O or H_2O (with Li_2SO_4 electrolyte and using the electrode configuration of Pons and Fleischmann) show a near-surface enrichment of Rh and Ag as detected by X-ray photoelectron spectroscopy (XPS). Rh and Ag are present as impurities in the starting Pd material but at levels (50 and 100 ppm, respectively) well below the XPS detection limit. The surface concentration of Rh increases as a function of total accumulated electrolytic charge and reaches a maximum of ~4 atom % relative to Pd. It is demonstrated that Rh and Ag are not electrodeposited at the Pd surface but rather must derive from the palladium itself. This phenomenon is most likely due to surface segregation of the Rh and Ag impurities under the forcing (current and time) conditions of the long-term (1–4 week) electrolyses as palladium deuteride or palladium hydride forms. An estimated segregation energy (ΔG) of 17 kJ/mol for Rh and 11 kJ/mol for Ag is obtained, derived from a chemical potential–driving force resulting from changes in the palladium matrix as the deuteride (hydride) phase forms.

INTRODUCTION

Our exploration of the provocative experiment of Fleischmann, Pons, and Hawkins (1) has concentrated on the surface analysis of Pd foils after their use to electrolyze D_2O or H_2O solutions (2–4), rather than to focus on analytical determinations of the expected physical signatures or chemical byproducts of the fusion reaction of deuterium with deuterium. The possibility of products created from reactions of palladium with nuclear byproducts, however, led us to look deliberately for low levels of Rh and Ag in the palladium after electrolysis of D_2O.

Rh and Ag are tantalizingly close in atomic number to Pd—one down and one up, respectively. These elements can form from the interaction of palladium with some of the expected products of D–D fusion, e.g., by neutron reactions with Pd isotopes (5); see Table I. The decay products of most of these neutron-activation reactions are the stable Pd isotopes; however, the decay products of the ^{103}Pd and ^{109}Pd radioisotopes are the stable isotopes ^{103}Rh and ^{109}Ag, respectively (6, 7).

As we describe in this paper, low-level Rh and Ag impurities, present in the native Pd, were observed at significantly higher levels at the surface after electrolysis of either D_2O or H_2O, as determined by X-ray photoelectron spectroscopy (XPS). The increased concentration of these elements at the surface as a result of electrolysis, independent of the nature of the hydrogen isotope, implies that unanticipated and substantial

---

Table I. Neutron Activation Reactions of Pd Isotopes with 14-MeV Neutrons and Thermal Neutrons (5)

nuclear reaction	cross section, σ/b	$t_{1/2}{}^a$
fast		
$^{104}Pd(n,p)^{104}Rh$	0.13	44 s
$^{105}Pd(n,p)^{105}Rh$	0.70	36 h
$^{110}Pd(n,\alpha)^{107}Rh$	0.014	4 min
$^{110}Pd(n,2n)^{109}Pd$	2	13.6 h
$^{108}Pd(n,\alpha)^{105}Ru$	0.0022	4.5 h
thermal		
$^{102}Pd(n,\gamma)^{103}Pd$	4.8	17 days
$^{108}Pd(n,\gamma)^{109}Pd$	7.7	13.6 h
$^{110}Pd(n,\gamma)^{111}Pd$	0.4	22 min

^{a} Half-life.

---

movement of metallic impurities inherent to the palladium occurs during the electrolyte formation of palladium deuteride or palladium hydride.

EXPERIMENTAL SECTION

Materials and Electrolytic Conditions. All experiments described in this paper were run with samples cut from one piece of Pd foil (0.127-mm thick) obtained from the historical supply of precious metals in the electrochemistry group at the Naval Research Laboratory. X-ray diffraction (Philips/Norelco Model XRG 6000 X-ray diffractometer) of this foil showed that it was oriented primarily in the ⟨200⟩ direction.

The Pd-foil cathode was cut in the shape of a rectangular strip; a spot-welded contact was made to 0.5-mm-diameter Pd wire (Aldrich, 99.99% pure). Prior to electrolysis, the dull gray Pd foil was cleaned in freshly prepared 1:1 HCl/HNO_3 as follows: the Pd strip was gently moved through the acid for 90 s and then sonicated three times in fresh H_2O; this step was repeated twice; finally the foil (now shiny and showing visible grains) was sonicated in the solvent of electrolysis.

The palladium cathode (of varying area, >1 cm²) was concentrically surrounded by an anode of platinum wire (Alfa, 5 N pure) wrapped around the outside of a glass-rod cage, as in the Pons and Fleischmann design (1, 8). Unless the anode symmetrically surrounds the palladium cathode, electrolysis merely achieves the diffusion of deuterium through (and out of) palladium. The electrolyte solution was 0.1 F Li_2SO_4 (anhydrous, Alfa) in one of two sources of 99.9% pure D_2O (MSD Isotopes or Cambridge Isotope Laboratories, used as received) or H_2O (triply distilled from quartz).

A single experiment was prepared under dry conditions with LiOD electrolyte: previously unopened D_2O (Cambridge Isotope Laboratories) was placed in a drybox (Vacuum Atmospheres: He atmosphere at < 1 ppm H_2O) and used to prepare 0.1 F LiOD from Li metal ribbon (Alfa). The cell was assembled in the drybox and removed for electrolysis.

The Pd was charged at a constant current of 10 mA/cm² by using the galvanostatic mode of a EG&G PAR Model 173 potentiostat/galvanostat; due to the thinness of the foil, the time calculated to fully charge the palladium was less than 1 day. The cell voltage was measured by connecting the reference and auxiliary electrode leads to the electrometer. After initial charging, some cathodes were charged at 50 or 140 mA/cm². X-ray dif-

---

*Author to whom correspondence may be addressed.

Table II. Bulk Analysis of Impurities in Pd Foil

element	concn, ppm	element	concn, ppm
Pt	200	Si	20–40
Rh	50	B	tr
Ag	100	Al	tr
Cu	50	Fe	tr
Mn	10–15	Ru	a
Ni	200–300	Mg	a

a Element is not present at the limit of detection.

fraction of the electrolyzed Pd foil showed that the lines for palladium were gone and lines for a palladium deuteride phase were present.

Elemental Analyses. Bulk analyses of the Pd foil before and after electrolysis in D_2O or H_2O were performed at the National Institute of Standards and Technology, using atomic emission spectroscopy (Jarrell-Ash Model 750 spectrophotometer) by ASTM Suggested Method 11-22 (9). The Pd samples (5 ± 1 mg pieces) were loaded into graphite-cup electrodes and diluted with 5 mg of pure graphite. The samples were vaporized and excited with a 7.5-A dc arc. Emission lines from 230 to 350 nm were photographically recorded on Spectrum Analysis No. 1 plates in the 3.4-m Ebert spectrograph. Qualitative and quantitative identifications of elements were made by visually matching multiple characteristic lines from a set of standards containg 49 common elements of known concentration in a 99.999% Pd sponge.

Elemental analyses of surface species via XPS were performed with a Surface Science Instruments Model SSX-100-03 X-ray photoelectron spectrometer with a small-spot capability using an Al anode and at pressures < 5 × 10⁻⁹ Torr. Binding energies are referenced to trace, adventitious carbon (C1s = 284.6 eV). For quantitation, peaks were fit by using a χ^2-minimization routine. Peak positions, heights, and widths were assigned initially by graphic editing. The relative areas of the elemental lines were corrected for cross-sectional and instrumental factors.

Outgassing from foils analyzed immediately after electrolysis produced analyzer–chamber pressures of > 10⁻⁷ Torr; pump-down periods of > 12 h were required before the pressure dropped to a level suitable for operation of the spectrometer (<10⁻⁸ Torr). Mass spectral analysis of the gas phase imposed by outgassing from electrochemically generated PdD_x showed that the bulk of the pressure was due to m/z 4, with significant (>10⁻⁸ Torr) quantities of m/z 2, 3, 5, and 6 and peaks attributable to $H(D)_2O^+$.

The persistence of deuterium within the Pd can be illustrated by the sample run in $LiOD/D_2O$ for an accumulated charge of 1.3 × 10⁶ C. This sample was analyzed 32 days after electrolysis was terminated and still produced an m/z 4 signal of 1 × 10⁻⁹ Torr, from an instrumental background level of 10⁻¹¹ Torr.

Elemental analyses of the Li_2SO_4 solutions in D_2O were performed with inductively coupled plasma emission spectrometry and indicated no trace metallic impurities at ppm levels.

RESULTS

Bulk Analysis of Pd. Atomic emission spectroscopic analyses of Pd foil before and after electrolysis of either D_2O or H_2O showed essentially identical levels of metallic impurities in all cases. Table II lists the impurities observed for the Pd starting material; even the Pd foil electrolyzed for a total of 1.3 × 10⁶ C of charge exhibited the same levels of metallic impurities. The sum of these metallic impurities is less than 1000 ppm; thus, the Pd foil is about 99.9% pure with respect to the metallic elements.

Although soluble (or dissolvable) impurities present in (or from) the electrochemical cell are anticipated to electrodeposit at the surface of the cathode during the long-duration electrolyses necessary to explore the Fleischmann–Pons effect, such species were not present, in our experiments, in sufficient quantities to discriminate between the postelectrolysis concentration of an impurity relative to its initial bulk concentration. For example, although Pt was expected (and observed by XPS, see below) to deposit at the cathode during long-

duration electrolysis, the total postelectrolysis amount of Pt (electrodeposited Pt + bulk Pt impurity) was sufficiently less than the 500-ppm Pt standard such that the intensities of the emission lines for Pt were still best described by emission intensities obtained for the 200-ppm Pt standard in Pd, i.e., at the level observed for the starting Pd material (see Table II).

XPS Analysis. We chose a Li_2SO_4 electrolyte, which is a neutral-pH solution, rather than the strongly basic LiOD electrolyte used by Pons and Fleischmann (1, 8) and copied by most experimenters seeking to replicate their results. Reasoning that the pertinent half-cell electrochemical reaction, i.e., the reduction of D_2O at the cathode,

$$D_2O + e^- \rightarrow D^{\bullet} + OD^- \tag{1}$$
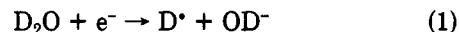
occurs in both neutral and basic solutions, we opted for the less resistive and lower etchant electrolyte. As a consequence of this choice, we dissolved less of our glass cell over the days and weeks of electrolysis; thus, our surfaces are not a primary reflection of the silicon, alkali-metal, alkaline-earth, and boron components of glass. Although these species can be observed by XPS after several days of electrolysis, a Pd signal was obtained for all samples, except for the single instance of $LiOD/D_2O$ electrolysis. This permitted direct XPS analysis of the surface without ion etching or sputtering.

XPS survey scans (0–1000 eV) of foils from both D_2O and H_2O experiments indicated the presence of Pd, Pt, C, and O and traces of Cu, Ni, Fe, Zn, Si, Na, and Mg (3). Survey scans of the as-received Pd foil or the 1:1 HCl/HNO_3-cleaned Pd foil show no trace of Pt, Cu, Ni, Fe, Zn, Si, Na, or Mg. Platinum is expected to be present on the surface of the Pd foil after long-duration electrolysis because Pt oxidatively dissolves from the anode and electroplates at the Pd cathode. Pt has been observed on the surface of Pd used to electrolyze $LiOD/D_2O$ solutions by XPS (10) and EDAX (11) analysis. Based on our results, this process also occurs from pH-neutral solutions.

Not unexpectedly, the purity of the electrolyte and the electrode and cell materials is critical. Si, Na, and Mg derive from the borosilicate glass of the electrochemical cell. The source of the Cu, Ni, and Fe present at the surface after electrolysis is less clear but is probably related to contact corrosion. The presence of Zn at the surface of Pd after electrolysis has been linked to varying low levels in the as-obtained D_2O (10).

Table III consolidates the binding energies and atom percent ratios obtained for HCl/HNO_3-cleaned Pd foil before and after electrolysis in D_2O and H_2O. The observed binding energies of the characteristic lines for Pd ($Pd3d_{5/2}$: 335.1 eV) and Pt ($Pt4f_{7/2}$: 71.0 eV) are consistent with their presence as metallic Pd(0) and Pt(0) (12). The surface concentration of Pt relative to Pd increases as the amount of accumulated charge increases. This can be clearly seen in Figure 1, in which the atom percent of Pt relative to Pd is plotted as a function of total accumulated charge.

The amount of Pt at the Pd surface does not seem to be dependent on whether the electrolysis is performed in light or heavy water but does accrue with increased electrolytic charge. This conforms with a mechanism dependent on oxidative dissolution of the Pt anode and subsequent plating as Pt metal at the Pd cathode. This process would occur in both H_2O and D_2O.

Multiple signal-averaged, high-resolution scans revealed the presence, after electrolysis, of Rh and Ag at concentrations of several atom percent relative to Pd. The presence of these species came as a surprise, as, at 50- and 100-ppm levels, respectively, in the bulk Pd, they are below the limit of detection of XPS. Even trace signals for Rh and Ag cannot be observed by multiple, signal-averaged, high-resolution scans

Table III. High-Resolution XPS Analysis of 127-μm Pd Foil before and after Electrolysis in D_2O or H_2O^c

sample	sample no.	accum charge, 10^3 C	no. of times $i \to 0$	binding energy, eV				atom % rel to Pd^a			
				Pd3d$_{5/2}$	Pt4f$_{7/2}$	Rh3d$_{5/2}$	Si2p	Pt/Pd	Rh/Pd	Ag/Pd	Na/Si
Pd foil cleaned in 1:1 HCl/HNO$_3$	1	0	0	335.4	---	---		0	0	0	
	2	0	0	335.3	---			0			
	3	0	0	335.2	---	---		0	0		
				335.3 ± 0.1							
cleaned Pd foil electrolyzed in 0.1 F Li$_2$SO$_4$/D$_2$O	4	>8.4	5	335.0	70.7			10.3			
	5	23.1	1	335.8	71.6	307.0		2.1	0.8		
	6	>39.5	11	335.3	71.2	306.5	---	11.2	1.1	1.1	
	7	67.3	2	334.9	70.9	306.6	tr	12.8	4.0		
	8	127.2	3	335.3	71.2	306.2	102.7	21.8	3.8	0.9	0
	9	254.5	4	335.0	71.1	306.8	102.3	38.8	3.5	1.2	3.05
				335.2 ± 0.3	7.71 ± 0.3	306.6 ± 0.3	102.5 ± 0.2			1.1 ± 0.1	
cleaned Pd foil electrolyzed in 0.1 F LiOD/D$_2$O	10	1336	2	---	70.8	---	102.0	und	und	und	1.47
no. 10 cleaned in 1:1 HCl/HNO$_3$	11	1336	2	334.9	---	---	---	0	0	0	und
cleaned Pd foil electrolyzed in 0.1 F Li$_2$SO$_4$/H$_2$O	12	1.6	1	335.1	71.1			0.1	0		
	13	11.2	2	334.9	70.8	306.4		1.8	1.3		
	14^b	40.2	3	334.8 ± 0.2	71.1 ± 0.1	305.6 ± 0.1	102.4 ± 0.2	3.9 ± 0.4	1.3 ± 0.6	1.2	21 ± 2
				334.9 ± 0.3	71.0 ± 0.2	305.9 ± 0.5					

^{a} Atom % defined as Pt4f$_{7/2}$/Pd3d; Rh3d$_{3/2}$/Pd3d; Ag3d$_{5/2}$/Pd3d; Na1s/Si2p. ^{b} Sample reanalyzed 1 month later to obtain high-resolution scan of Ag3d region; values averaged for all other regions. ^{c} Blank space: region not scanned. ---: region scanned, no peak. und: the relative area of Pd is nearly 0, so the calculation is undefined.
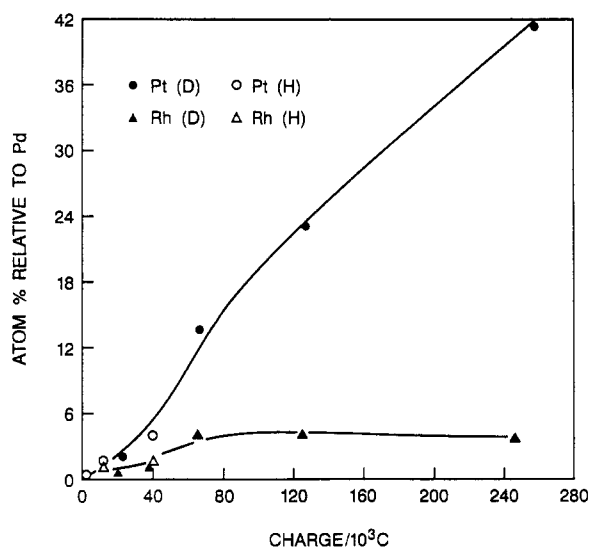

Figure 1. Atom percent (relative to Pd) Pt and Rh obtained from XPS analysis of Pd foils after electrolysis in D_2O and H_2O as a function of total accumulated electrolytic charge; the solid curves are drawn to guide the eye.

of the Rh3d and Ag3d energy ranges for cleaned, but non-electrolyzed, Pd foil (see Figures 2B and 3A). As 99.999% Pt was used for the anode, it is improbable that Ag and Rh are present at sufficient levels in the Pt to account for concentrations of several atom percent at the Pd surface via anodic dissolution of the Pt (and associated impurities) and cathodic plating of the Pt-associated impurities. Other evidence used to rule out electrodeposition of Ag and Rh will be described below.

The determination of Rh by XPS—in this particular chemical system—is complicated by neighboring signals for species present on the Pd surface, usually at higher concentrations than the Rh. Figure 2 shows how, after electrolysis, the presence of the Rh3d$_{5/2}$ line is obscured by the Mg KL$_{23}$L$_{23}$ Auger line and the Rh3d$_{3/2}$ line is surmounted by the Pt4d$_{5/2}$ line. The resolution of the Rh3d$_{3/2}$ line from its interferant is the more apparent, so this line was used to determine the amount of Rh at the surface and, using the known 3d$_{3/2}$–3d$_{5/2}$
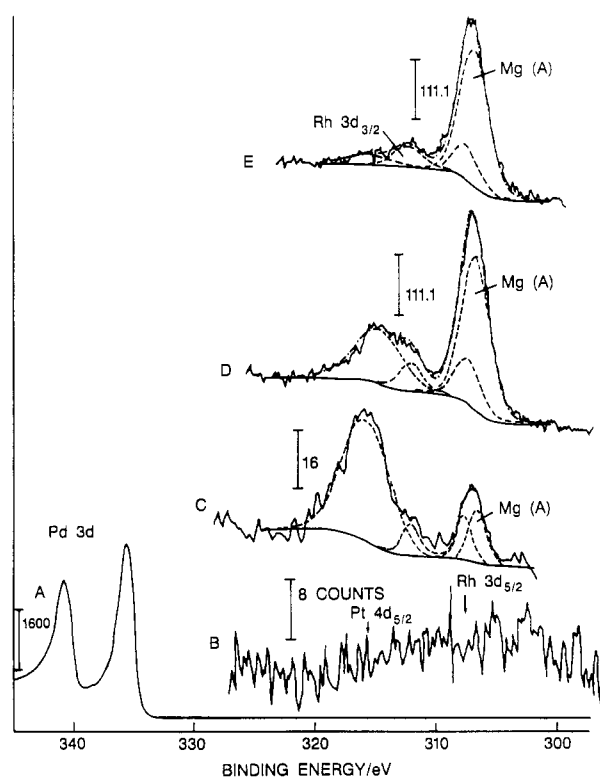

Figure 2. High-resolution scans of the energy region encompassing Pd3d, Pt4d, Rh3d, and Mg KL$_{23}$L$_{23}$ Auger lines, including the deconvoluted spectrum for the envelope containing the Pt4d$_{5/2}$, Rh3d$_{3/2}$, Rh3d$_{5/2}$, and Mg Auger lines for the following samples: (A and B) Pd after etching in 1:1 HCl/HNO$_3$; (C) PdH$_x$ (sample 14); (D) PdD$_x$ (sample 7); (E) analysis of lightly scratched region of sample 7. See Table III for electrolytic conditions.

separation for Rh of 4.75 eV (12), the binding energy for Rh3d$_{5/2}$. The average binding energy of 306.6 eV thus determined is consistent with metallic Rh(0) (12).

Figure 1 and Table III include the atom percent Rh as a function of total accumulated charge. It can be seen that the low level of Rh appears to plateau at approximately 4 atom % relative to Pd before the amount of charge passed becomes
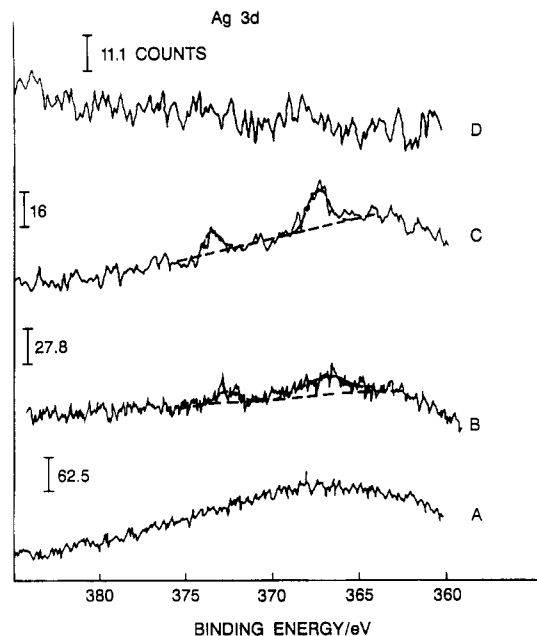
Figure 3. High-resolution scans of the Ag3d region for the following samples: (A) Pd after etching in 1:1 HCl/HNO₃; (B) PdH$_x$ (sample 14); (C) PdD$_x$ (sample 8); (D) PdD$_x$ (sample 10). See Table III for electrolytic conditions.

too great to reasonably determine the Rh, due to the greater amount of electrodeposited Pt. The Ag signal is minimal and constant at approximately 1 atom %; the $3d_{5/2}$–$3d_{3/2}$ spin-orbit doublet has a separation and binding energy consistent with Ag (12). As with the electrodeposited Pt, the amount of Rh or Ag at the surface does not appear to be dependent on the isotopic identity of the aqueous solution.

The determination that the Rh and Ag found at the surface after electrolysis do not derive from electrodeposition can be found in Figures 2 and 3. A portion of the Pd-foil sample was lightly scratched to expose subsurface Pd, and by taking advantage of the small-spot capability of our spectrometer, a spectrum could then be obtained centered on this scratch. The resulting spectrum becomes a composite of surface and subsurface species and is enriched in Pd relative to the spectrum obtained for an unscratched region of the same sample. Qualitatively, species present due solely to electrodeposition should appear diminished, while species enriched in the near-surface layer should appear relatively unchanged.

The result for Rh can be seen by comparing Figure 2D (unscratched) and 2E (scratched) for sample 7 (see Table III). The signal for Pt4d$_{5/2}$, due to electrodeposited Pt, is markedly lowered when focused on the scratched, bulk Pd-rich region, while the signal for Rh3d$_{3/2}$ can be seen to remain essentially unchanged. The low-level signal observed for Ag on Pd electrolyzed in aqueous Li₂SO₄ (Figure 3B and 3C) is not present for the Pd foil used to electrolyze LiOD/D₂O—the one sample with sufficient electrodeposited species, including Pt, to block the Pd3d signal (Figure 3D and Table III). Consequently, the Ag present at the surface of Pd used to electrolyze LiSO₄ solutions also does not derive from electrodeposited impurities but is connected to the presence (and absence) of the Pd.

DISCUSSION

The observation that the surface concentrations of Rh and Ag reach some constant level with accumulated electrolytic charge but do not further increase, even after extensive electrolysis ($>0.25 \times 10^6$ C), implies that their presence may be due to migration from the Pd interior during the long times of the deuteriding/hydriding reaction. With such a mecha-

nism, a natural limit to the surface concentrations of Rh and Ag would result as a function of their concentration in the bulk material and their diffusivity characteristics in palladium and palladium deuteride (hydride).

Silver forms a continuous series of solid solutions with palladium (13, 14) through the entire temperature range, while rhodium forms solid solutions with palladium above 850 °C (14), so, it is somewhat unexpected that either element would readily move through Pd to segregate in a near-surface layer. In hindsight, forced transport of even compatible solute atoms may indeed be possible during the great buildup of D⁺ (H⁺) in the palladium lattice compelled by electrolyzing D₂O (H₂O) at Pd in a symmetric electric field over the long times of these electrolyses, especially in view of the phase changes occurring as palladium deuteride (hydride) forms.

Previous measurements of the diffusivity of hydrogen in solid solutions of palladium and rhodium (15, 16) involved the use of the alloy as a membrane through which hydrogen, electrochemically generated at one face of the membrane, diffused to the opposite side. The lowest concentration of Rh in Pd studied in Yoshihara and McLellan's membrane experiments was 3 atom %, and electron-probe microanalysis of selected Pd–Rh membranes after hydrogen-diffusion studies did not reveal compositional inhomogeneities (16). In Pd membrane experiments, however, the hydrogen-to-palladium loading will not reach a level consistent with the formation of the β-phase *throughout the entire material*, so the physical nature achieved in these membrane experiments cannot be directly compared to that obtained for palladium charged with deuterium or hydrogen following Fleischmann–Pons conditions. The Pd membranes are also not maintained at or beyond the β-phase for the time durations usual for Fleischmann–Pons experiments.

The segregation of solutes to the surface of solids is a well-studied phenomenon by surface analysis (17). Typically, segregation results after forceful treatment of the solid, e.g., after exposure to temperatures consistent with annealing (17, 18) or after fracturing (17, 19), or during corrosive oxidation (17) or energetic ion bombardment (17, 20) of the surface. When surface species are removed, and at different rates, the difference in the chemical potential of a solute species at the surface from its chemical potential in the bulk ($\mu_i^{0,\Phi} \neq \mu_i^{0,B}$; for the ith solute, where Φ and B refer to surface and bulk, respectively) leads to surface segregation.

In the case of radiation-enhanced segregation of a Pd–Pt alloy, where the Pd is preferentially sputtered, Du Plessis, Van Wyk, and Taglauer determined a segregation energy (ΔG) from the Langmuir–McLean equation,

$$\frac{X_i^{\Phi}}{1 - X_i^{\Phi}} = \frac{X_i^{B}}{1 - X_i^{B}} \exp(\Delta G/RT) \qquad (2)$$

where X_i represents the mole fraction of solute i in the bulk (B) and at the surface (Φ) relative to the solvent. For ion-bombardment energies of 1 keV, the segregation energy decreased from 8 to 2 kJ/mol as the Pd concentration increased from 10 to 90 atom % (20).

In the PdH$_x$ or PdD$_x$ system, we have no evidence for the loss of either Pd or solute atoms to the solution during the electrolytic formation of the hydride or deuteride. In this system, we postulate that segregation occurs because the solutes (Rh and Ag) are now dissolved in a solvent undergoing a phase transformation. The palladium deuteride (hydride) forms first at the solid–liquid interface and, with continuing electrolysis and concomitant diffusion of D⁺ (H⁺) inward, transforms the bulk.

We postulate that the difference in the chemical potential of Rh (Ag) in the interior from that of Rh (Ag) at the interface as the Pd phase is transformed to PdD$_x$ or PdH$_x$ now becomes

the driving force for surface segregation of Rh and Ag in this system. By using the Langmuir–McLean equation (2), the ΔG for segregation can be calculated for these low-level solutes. By using the bulk concentrations (50 ppm Rh and 100 ppm Ag, relative to bulk Pd) for X^B and the XPS-derived surface concentrations (4 and 1 parts per hundred (pph), respectively, relative to surface Pd) for X^Φ, surface segregation energies at 25 °C of 17 kJ/mol for Rh and 11 kJ/mol for Ag are obtained.

The segregation energies estimated above follow the general trend to higher values for lower concentrations of solute, as observed in the Pd–Pt system (20). The values for ΔG are lower limits at best in that the Langmuir formulation would strictly be applied to a surface coverage and not the near-surface concentration derived from the XPS measurement and in that surface segregations driven by the usual and more extreme treatments (heat, ion bombardment, etc.) typically predominate in the first layer (21).

Based on 2-fold greater presence in the bulk and a 4-fold lower surface presence, it is clear that Ag is less amenable to migration than is Rh. This preference for surface segregation agrees with the continuous solid solubility of Ag in Pd–Ag alloys (13, 14) and the trend for Rh-enriched regions in Pd–Rh alloys (14).

Hydrogen-induced fracturing has been observed after hydride formation in a titanium alloy (22), and while fracturing is a plausible mechanism for segregation phenomena, scanning electron micrographic analysis of these and related samples has not indicated severe cracking or fissuring at the surfaces of our electrochemically prepared samples (2–4). At this time, the chemical potential–driven segregation of Rh and Ag seems the best candidate mechanism, with transport most likely occuring along grain boundaries.

An estimation of the Rh concentration that would be obtained if all the Rh moved into the XPS analysis volume illustrates the magnitude of this segregation. For example, in a reservoir volume of Pd beneath a 1-mm analysis spot, to half the depth of the foil (half because the impurities can move to either face of the foil in the symmetric field), if the 50-ppm bulk Rh impurity is crammed into an XPS interfacial volume (1 mm wide and 12.5 nm deep—i.e., the XPS information depth or 5 times the photoelectron escape depth), a Rh:Pd concentration of 26 atom % would result (23), rather than the ~4 atom % actually obtained. This estimate shows that a high degree of segregation occurred.

The near-surface nature of the Rh and Ag enrichment can be confirmed by the acid-etch treatment of sample 10. After removing on the order of micrometers of material from the surface of this foil, XPS analysis showed the absence of the electrodeposited impurities (e.g., Pt, Si, Na, Mg). Signal-averaging 25 high-resolution scans of the Ag3d and Rh3d regions indicated no detectable quantities of Ag or Rh; see data for sample 11, Table III.

A diffusion coefficient for the transport of Rh to the face of the Pd foil can be estimated from $d \sim (Dt)^{1/2}$. From Figure 1, it can be seen that the steady-state level of ~4 atom % is reached for the PdD_x sample (no. 7) that accumulated 67.3 $\times$ 10^3 C of charge. The total time for this charge accumulation was 4.5×10^5 s. Again, moving the Rh half the depth of the foil (i.e., $d = 63.5\ \mu m$) in 4.5×10^5 s yields an estimated diffusion coefficient of 9×10^{-11} cm²/s.

The magnitude of the diffusion coefficients observed for the bulk diffusion of metals in metals varies greatly, e.g., the diffusion coefficient of Au in Ag (Ag–8% Au)—another fcc continuous solid solution (14)—is on the order of 10^{-11} cm²/s, but this rate of diffusion required an elevated temperature of 654 °C (24), while that obtained for the diffusion of the only slightly soluble Ag in Pb is on the order of 10^{-10} cm²/s at 88

°C (25). Our estimated diffusion coefficient at room temperature is on the order of 10^{-10} cm²/s; this indicates that the segregation observed for low levels of Rh in highly deuterated Pd is more similar to that of a binary system of low solubility, such as Ag in Pb (14, 25), rather than that more typical of binary alloys forming continuous solid solutions.

The presence of Rh and Ag as low level bulk impurities in the starting Pd material rather clouds the intriguing possibility of their creation by reaction of palladium isotopes with nuclear byproducts—as does the hydrogen-isotope-independent segregation of Rh and Ag. The most plausible mechanism remains chemical potential–driven migration under the forcing conditions (time and current) of electrolysis as the palladium deuteride (hydride) phase forms rather than one based on nuclear chemistry. Our willingness to look for secondary products from reactions of palladium isotopes with possible nuclear byproducts permitted, however, the also interesting observation of surface segregation of nearly ideal solutes during reductive electrochemical treatment of the palladium solvent.

LITERATURE CITED

(1) Fleischmann, M.; Pons, S.; Hawkins, M. J. Electroanal. Chem. 1989, 261, 301–308; 1989, 263, 187–188 (errata).
(2) Rolison, D. R.; Trzaskoma, P. P. J. Electroanal. Chem. 1990, 287, 375–383.
(3) Rolison, D. R.; O'Grady, W. E.; Doyle, R. J., Jr.; Trzaskoma, P. P. Proceedings of the 1st Annual Conference on Cold Fusion, Salt Lake City, UT, March 28–31, 1990; pp 272–280.
(4) Trzaskoma, P. P.; Rolison, D. R.; Vardiman, R. G. Applications of Surface Analysis Methods to Environmental/Materials Interactions; The Electrochemical Society: Pennington, NJ, in press.
(5) Taylor, D. Neutron Irradiation and Activation Analysis; Van Nostrand: Princeton, NJ, 1964.
(6) Strominger, D.; Hollander, J. M.; Seaborg, G. T. Table of Isotopes. Rev. Mod. Phys. 1958, 30, 585–904.
(7) Chart of the Nuclides; United States Atomic Energy Commission: Washington, DC, 1965.
(8) Fleischmann, M.; Pons, S.; Anderson, M. W.; Li, L. J.; Hawkins, M. J. Electroanal. Chem. 1990, 287, 293–348.
(9) Semiquantitative Spectrographic Analysis of Miscellaneous Materials by the Graphite Dilution Technique. Methods Anal. Spectrosc. 1987, 8.
(10) Ulmann, M.; Liu, J.; Augustynski, J.; Meli, F.; Schlapbach, L. J. Electroanal. Chem. 1990, 286, 257–264.
(11) Divisek, J.; Fürst, L.; Balej, J. J. Electroanal. Chem. 1990, 278, 99–117.
(12) Wagner, C. D.; Riggs, W. M.; Davis, L. E.; Moulder, J. F.; Muilenberg, G. E. Handbook of X-ray Photoelectron Spectroscopy; Perkin-Elmer Corp., Physical Electronics Division: Eden Prairie, MN, 1979.
(13) Hansen, M.; Anderko, K. Constitution of Binary Alloys; McGraw-Hill: New York, 1958.
(14) Binary Alloy Phase Diagrams, 2nd ed.; Massalski, T. B., Ed.; ASM International: Materials Park, OH, 1990.
(15) Artman, D.; Flanagan, T. B. J. Phys. Chem. 1973, 77, 2804–2807.
(16) Yoshihara, M.; McLellan, R. B. Acta Metall. 1986, 34, 1359–1366.
(17) Ferguson, J. F. Auger Microprobe Analysis; Adam Hilger: Bristol, 1989; Chapter 12.
(18) Peacock, D. C. Appl. Surf. Anal. 1986, 26, 306–316; 1986, 27, 58–70.
(19) Wild, R. K. Mater. Sci. Eng. 1980, 42, 265–271.
(20) Du Plessis, J.; Van Wyk, G. N.; Taglauer, E. Surf. Sci. 1989, 220, 381–390.
(21) Buck, T. M. In Chemistry and Physics of Solid Surfaces; Vanselow, R., Howe, R., Eds.; Springer-Verlag: Berlin, 1982; Vol. 4, pp 435–464.
(22) Peterson, K. A.; Schwanebeck, J. C.; Gerberich, W. W. Metall. Trans. A 1978, 9A, 1169–1172.
(23) The estimation of the expected Rh atom % for complete migration is determined by moving the amount of Rh at a concentration of 50 ppm

from the bulk reservoir volume to an interfacial region beneath a 1-mm spot (r = 0.05 cm). This requires a calculation of the number of Pd atoms in this reservoir volume: mass Pd = $(\pi r^2)d$ cm^3 × 11.4 g/cm^3 = 5.7 × 10^{-4} g, where d is half the total thickness of the foil (63.5 × 10^{-4} cm) and the density of Pd at 22.5 °C is used.

no. of Pd atoms = (mass of Pd/atomic weight of Pd)N_A =

3.2 × 10^{18} atoms

no. of Rh atoms = 50 × 10^{-6}(3.2 × 10^{18}) = 1.6 × 10^{14} atoms

The interfacial XPS information depth is 12.5 nm (5 × 2.5 nm, the photoelectron escape depth), so the Rh atoms are placed into the new volume of Pd (where d = 12.5 nm and r = 0.05 cm):

% Rh = {1.6 × 10^{14} atoms/[($\pi r^2)d$ cm^3 ×

11.4 g/cm^3](N_A/atomic weight of Pd)}100

% Rh = (1.6 × 10^{14} atoms/6.2 × 10^{14} atoms)100 = 26%

(24) Mallard, W. C.; Gardner, A. B.; Bass, R. F.; Slifkin, L. M. *Phys. Rev.* **1963**, *129*, 617–625.
(25) Amenzou-Badrour, H.; Moya, G.; Bernardini, J. *Acta Metall.* **1988**, *36*, 767–774.

Constant Potential Amperometric Detection of Underivatized Amino Acids and Peptides at a Copper Electrode

Peifang Luo, Fuzhen Zhang, and Richard P. Baldwin*

Department of Chemistry, University of Louisville, Louisville, Kentucky 40292

Direct detection of underivatized amino acids and peptides can be carried out via oxidation at copper electrodes. Two different oxidation processes are possible, depending on the applied potential and the prevailing solution conditions. The first, which occurs optimally in neutral or slightly basic solution at approximately 0.0 V vs Ag/AgCl, is related to complexation reaction between the amino acid analyte and Cu(II) from the passivated electrode surface. The second mechanism, which occurs optimally under strong alkaline conditions in the +0.4–0.8-V range, appears to involve the electrocatalytic oxidation of the amino acid species. Of the two, the latter process was the more attractive for constant potential amperometric detection in flow injection and liquid chromatography applications as it allowed detection down to the 1–10 pmol levels for most amino acids and simple peptides. Furthermore, the Cu electrode response was comparatively long-lived, with single-electrode surfaces typically showing analytically useful activity for periods as long as 2 weeks.

INTRODUCTION

Over the past decade, numerous procedures involving high-performance liquid chromatography (HPLC) have been successfully developed for the determination of amino acids, peptides, and related compounds (*1*, *2*). In these efforts, several different instrumental techniques, including, among others, UV–visible absorption, fluorescence, and mass spectrometry, have been utilized for the detection of these compounds following the HPLC separation. Nevertheless, there still remains a lack of reasonably simple and sensitive detectors that do not require prior formation of derivatives to enhance the absorptivity, volatility, etc., over that of the parent amino acids.

An attractive detection possibility for amino acids might be provided by electrochemistry following liquid chromatography (LC–EC). However, only a few amino acids—most notably, tyrosine, tryptophan, methionine, and cysteine—are electroactive at modest potentials at either conventional (*3–9*) or chemically modified (*10–12*) electrodes. Therefore, the

direct detection of underivatized amino acids by electrochemical means has been very limited in its useful applications, and the vast majority of the work reported to date in this area has also employed some form of chemical, photochemical, or radiochemical derivatization (*3*). An effective way around this difficulty is provided by switching from the carbon-based electrodes conventionally employed in LC–EC to metallic electrodes exhibiting a greater degree of activity toward amino acid oxidation. For example, Johnson and co-workers have recently reported the detection of trace amounts of underivatized amino acids with systems using gold and platinum electrodes (*13–15*). The most serious drawback of these noble-metal electrodes is that they are subject to rapid surface fouling and, as a result, require a continuously pulsed potential wave form for stable, long-term operation. Alternatively, constant potential detection of amino acids has been achieved by oxidation at non-noble transition-metal electrodes such as Ni (*16*) and Cu (*17–20*). With the former, the response is electrocatalytic in nature, involving the electrochemical formation of a Ni(III) surface species and its subsequent oxidation of the amino acid. For Cu electrodes, on the other hand, the mechanism has been shown to be complexation-based, utilizing the chelating ability of the amino acids toward Cu(II) to increase the electrochemical dissolution of the electrode substrate and thereby generate a proportionate increase in the anodic current observed.

Our previous work with Cu-based electrodes for the amperometric detection of carbohydrates (*21–24*) demonstrated the utility of an electrocatalytic oxidation of these compounds at copper electrodes and prompted us to investigate whether such a catalytic mechanism might be extended to a wider range of analytes including, in particular, the amino acids. Earlier, mostly voltammetric studies by Hampson et al. (*25*, *26*) clearly indicated that such a process, requiring modest positive potentials in strongly alkaline solution, does indeed occur for alanine and several other amino acids. In the work reported here, we have experimentally verified the electrocatalytic oxidation of amino acids and peptides at the copper electrode and have shown it to operate distinctly from the complexation scheme reported earlier (*17*). In addition, we report an initial evaluation of the copper electrode as a cat-